Nanoparticle Formation via Copper (II) Acetylacetonate Vapor Decomposition in the Presence of Hydrogen and Water

Albert G. Nasibulin, Esko I. Kauppinen,* David P. Brown, and Jorma K. Jokiniemi

VTT Chemical Technology, Aerosol Technology Group, P.O. Box 1401, FIN-02044 VTT, Finland

Received: April 17, 2001; In Final Form: August 20, 2001

Copper (II) acetylacetonate ($Cu(acac)_2$) vapor decomposition and subsequent copper and copper (I) oxide particle formation were studied in a vertical laminar flow reactor in the presence of hydrogen and water vapor in a nitrogen atmosphere. The presence of hydrogen does not significantly affect on the decomposition rate. The most reactive conditions for the precursor decomposition appear when water vapor is introduced into the system. A mechanism for $Cu(acac)_2$ decomposition in the presence of water has been proposed. The reaction pathway can be divided into three steps: formation of gaseous hydrate complex; a proton transition from the coordinated water to a ligand and further liberation in the form of gaseous acetylacetone; the partial destruction (oxidation) of the resulting ligands and reduction reaction of Cu^{2+} to Cu^0. The formation of copper particles leads to a surface catalytic reaction of the organic decomposition products. As a result of this reaction, low volatile long chain compounds containing ketone, alcohol, ester, and ether groups are formed. The crystallinity of the particles depends on the experimental conditions and changes from copper to copper (I) oxide when the precursor vapor pressure is decreased from $P_{Cu(acac)_2} = 6$ to 0.13 Pa at $t_{furn} = 432$ °C and the temperarture is increased to $t_{furn} = 705$ °C at $P_{Cu(acac)_2} = 6$ Pa. A qualitative thermodynamic explanation of the change of crystalline phases is proposed. Primary particle size distributions were measured at $t_{furn} = 432$ °C. The size of the particles is dependent on $P_{Cu(acac)_2}$; the geometric mean diameter of $D_p = 27.3$ nm (with geometric standard deviation of $\sigma_g = 1.34$) at $P_{Cu(acac)_2} = 6$ Pa, $D_p = 15.6$ nm ($\sigma_g = 1.35$) at $P_{Cu(acac)_2} = 1.9$ Pa, $D_p = 5.2$ nm ($\sigma_g = 1.33$) from TEM images and $D_p = 6.1$ nm ($\sigma_g = 1.35$) from DMA measurements at $P_{Cu(acac)_2} = 0.13$ Pa, and $D_p = 4.2$ nm ($\sigma_g = 1.19$) from DMA measurements at $P_{Cu(acac)_2} = 0.07$ Pa.

I. Introduction

β-Diketonate complexes are of growing interest due to favorable physical and chemical properties. Aside from the usage of these compounds as fuel additives and catalysts,[1] β-diketonate complexes also have been used as metal vapor sources. High volatility and low decomposition temperature of the compounds are useful quantities for industrial processes such as the chemical vapor deposition (CVD) of superconductive layers.[2] For the same reason, this class of compounds can be also used for another very important technological task—metallic particle synthesis. The production of metallic powders can be realized by means of the chemical vapor nucleation (CVN) method. When compared to physical methods of metallic particle synthesis, the obvious advantage of the CVN method is the possibility of producing particles at relatively low temperatures.[3−5] Thus, this is likely the least expensive of available methods for controlled aerosol particle production.

The task of our investigation is copper and copper oxide particle synthesis by the CVN method. The importance of producing copper and copper oxide particles is exemplified by applications for electronics, ceramics, thick/thin film applications, and many others[6,7] and as high surface area catalysts that are used in diverse chemical processes.[8−10] For this purpose, one of the best candidates among the β-diketonate compounds is copper (II) acetylacetonate ($Cu(acac)_2$) due to suitable equilibrium vapor pressure and low decomposition temperature (t_{dec}=286 °C). Other favorable aspects of the precursor are its commercial availability, its relatively low cost compared to the costs of other β-diketonate compounds, and its popularity as a precursor for CVD studies.[11−14]

Unfortunately, very little work has been devoted to copper and copper oxide formation using either β-diketonate complexes in particular or the CVN method in general. Okuyama et al.[15] used β-diketonate complexes of various metals for the gas-phase synthesis of the superconductive oxide particles of Bi, Sr, Ca, and Cu mixtures. Daroczi et al.[16] studied the production of copper and iron nanocomposites by thermal decomposition of copper ferrocyanide in an open vertical tube. Synthesis of copper and copper oxide particles using $Cu(acac)_2$ precursor has not been reported so far, except our recent research.[17] It was shown that copper and copper (I) oxide nanometer-size particles could be obtained by $Cu(acac)_2$ chemical vapor decomposition in an inert nitrogen atmosphere. The disadvantage was the need of relatively high temperature (705 °C) for complete precursor decomposition. It is well-known that using some suitable reagents can increase the decomposition rate at given temperature. According to the literature data for CVD studies,[2,18] the possible candidates for this purpose could be hydrogen, which participates in the reduction reaction of the precursor, and water, which forms hydrate complex with low decomposition temperature.

The goals of the current investigation are to study the influence of hydrogen and water on the decomposition of copper (II) acetylacetonate, to produce nanoparticles at a temperature as low as possible and ambient pressure, to characterize the

* To whom all correspondence should be addressed. Tel: +358 9 456 6165. Fax: +358 9 456 7021. E-mail: Esko.Kauppinen@vtt.fi.

10.1021/jp0114135 CCC: $20.00
Published on Web 10/24/2001

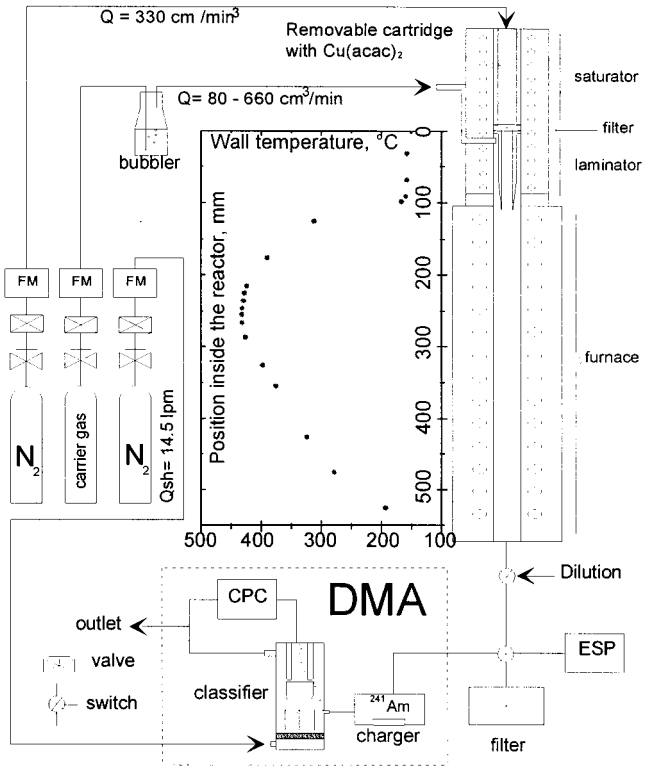

Figure 1. Schematic presentation of the experimental setup.

obtained nanoparticles synthesized under various reactor conditions, and to discuss the mechanisms of $Cu(acac)_2$ decomposition and subsequent nanoparticle formation on the basis of the experimental results.

II. Experimental Section

2.1. Materials. For the current investigation, a powder of copper (II) acetylacetonate (Aldrich Chemical Co., 97%) has been used as a precursor. Blocking of the flow due to the compaction of the $Cu(acac)_2$ powder in the saturator was prevented by using an inert chromatographic carrier, silicon dioxide (Balzers Materials, 99.9% with grain size of 0.2−0.7 mm). A mixture of 4 g (1.53×10^{-2} mol) of copper (II) acetylacetonate and 16 g (0.27 mol) of silicon dioxide has been used for saturation of the carrier gas in the saturator.

In our study, two kinds of gas carriers have been used. A mixture of nitrogen and hydrogen (AGA) with a mole component ratio of 93.0/7.0 was used to check the influence of the reducing conditions on $Cu(acac)_2$ decomposition and on the characteristics of formed particles. Pure nitrogen (AGA, 99.999 vol %) was selected for saturation of the stream by the precursor and in order to examine the precursor decomposition in the presence of water vapor. Distillated and deionized water (Alpha-Q, Millipore) was put in the bubbler to saturate the carrier gas and used as a reagent for the precursor vapor.

An organic solvent, toluene (Riedel-de Haën, 99.7%), was used for infrared analysis sample preparation.

2.2. Description of the Experimental Method. For the current investigations, a laminar vertical flow reactor has been designed and constructed. The experimental device consists of a saturator, a laminator, and a furnace (Figure 1). The saturator and the laminator have been made of stainless steel. A ceramic tube with internal diameter of 22 mm inserted inside the furnace (Entech, Sweden) has been used as a reactor.

During an experiment, two kinds of carrier gases have been simultaneously used. The first is inert nitrogen for saturation by $Cu(acac)_2$ vapor. The second carrier gas can be either pure nitrogen or a mixture of nitrogen and hydrogen (with a mole component ratio of 93.0/7.0) in order to check the possibility of the $Cu(acac)_2$ reduction reaction. Water vapor, when needed, is also introduced into the system for checking the possibility of reaction between the reagent and the precursor. A water bubbler at ambient temperature is used for this purpose. The mixture of nitrogen and a reagent (hydrogen and/or water) is introduced into the setup from the side and separated from the $Cu(acac)_2$ vapor flow by a 1 mm thickness stainless tube with internal diameter of 11 mm. Inside the furnace, the flows were mixed and then heated.

The flow rate was measured by a flow meter (DC-2, BIOS) and always referred to standard conditions ($t = 25$ °C, $P = 1$ atm). Temperatures were measured by nicrom−nickel thermocouples calibrated to an accuracy of 0.1 °C. The aerosol number size distributions in the range of 2−200 nm were measured by a differential mobility analyzer (DMA) system consisting of a charger, a classifier,[19] and a condensation particle counter (CPC, TSI 3027). An electrostatic precipitator (ESP, InTox products) was used to gather the aerosol particles on a carbon-coated copper grid (SPI Holey Carbon Grid). The morphology of the particles was studied with a field emission scanning electron microscope (SEM, Leo Gemini DSM982). Qualitative elemental analysis of the particles was carried out with an energy-dispersive X-ray spectrometer (EDS, Noran Voyager) connected to the SEM. The primary particle size and the crystallinity of the particles were investigated with a field emission transmission electron microscope (TEM, Philips CM200 FEG). Electron diffraction patterns and high-resolution TEM images were used for determination of the crystalline phase of particles. The samples for X-ray diffraction (XRD, Philips MPD 1880 powder X-ray diffractometer) spectrometry were collected on silver filter disks (Millipore AG4502500) and studied with Cu Kα (λ = 0.154 nm) radiation. Infrared (IR) spectra of samples were obtained by a Bruker Equinox 55 spectrophotometer (resolution 4 cm^{-1}) with IRScope II microscope and by using a Perkin-Elmer 1760X spectrophotometer. A Mettler Toledo TA8000 system equipped with a TGA850 thermobalance was used for thermogravimetric analysis (TGA). A gas downstream of the furnace was collected into a retort and then analyzed using a gas chromatography mass spectrometer (JEOL SX-102).

Inside the reactor, known wall temperature gradients have been maintained with three temperature profiles. One of these wall temperature profiles is shown in Figure 1. From the enclosed graph, one can find that the maximum measured wall temperature was maintained within 1 °C ($t = 431.5 \pm 0.5$ °C) at the distance of 255 ± 12 mm. Experiments were also performed with a similar wall temperature profile with temperature maxima at $t = 596.0 \pm 0.5$ and 705.0 ± 0.5 °C, where these conditions were valid at $x = 255 \pm 14$ and 255 ± 15 mm, respectively. In the following, those three temperature profiles will be referred to as 432, 596, and 705 °C.

Using of the removable cartridge with the precursor (Figure 1) allowed the determination of the $Cu(acac)_2$ vapor pressure downstream of the saturator. The vapor pressure was calculated from the known gas flow rate and the mass difference of the cartridge over a certain time interval. The $Cu(acac)_2$ pressure after the saturator is maintained equal to $P_{Cu(acac)_2} = 6 \pm 1$, 1.9 ± 0.3, 0.13 ± 0.02, and 0.07 ± 0.01 Pa. Thus, during the experiments, the temperature and the contents of vapor-gas phase are well controlled. The values of vapor pressure and concentration, given hereinafter, were calculated for gaseous species at

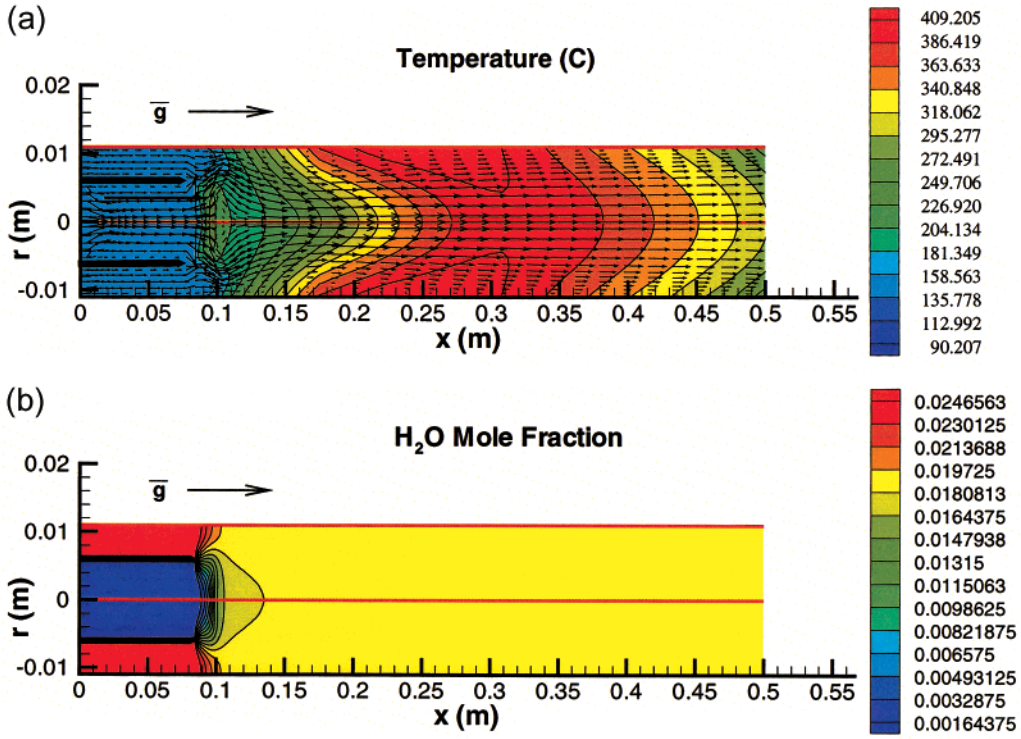

Figure 2. (a) Velocity vectors and contours of gas temperature for the $Cu(acac)_2-H_2O-N_2$ system and $t_{furn} = 432$ °C. (b) Contours of H_2O mass fraction for the $Cu(acac)_2-H_2O-N_2$ system and $t_{furn} = 432$ °C.

the entrance to the reactor, i.e., before mixing precursor and reagent flows.

2.3. Computational Fluid Dynamics Calculations. Computational fluid dynamics (CFD) calculations have been carried out to check the temperature and velocity profiles and mixing conditions of the species in the reactor. The gas-phase species transport and heat transfer calculated with the StreamWise CFD program[20] for two different experimental systems of $Cu(acac)_2-H_2-N_2$ and the $Cu(acac)_2-H_2O-N_2$. The flow is laminar and buoyant. Grid resolution studies show that a grid with 66×31 points is sufficient to resolve the phenomenon under consideration. The origin is chosen to be the outlet of the $Cu(acac)_2$ filter holder where the precursor is at known saturated conditions. The calculation is axisymmetric (since gravity is in the axial direction), which allowed the use of symmetry boundary conditions at the centerline. In addition to conservation of mass, momentum, and energy, two gas-phase species equations for N_2 and either H_2 or H_2O were solved. The presence of $Cu(acac)_2$ was neglected because of small fraction of the component in the gas phase (the precursor mole fraction was less 6×10^{-5}). Buoyancy effects are included in the calculation. Inflow boundary conditions on mole fractions of the various species, inflow velocity, pressure, and temperature are the same as those in the described experiments. Wall temperature boundary conditions are linearly interpolated from experimentally measured wall values. Inert wall boundary conditions have been used for the gas-phase species.

Results are shown for the $Cu(acac)_2-H_2O-N_2$ system only, though the behavior is similar in both systems. Figure 2a shows the heat transfer, velocity field, and the mixing of N_2 and H_2O in the reactor. The entire flow reaches a temperature of at least 398 °C, with the minimum peak temperature occurring along the centerline at $x = 0.34$ m. There are small recirculation regions at the centerline at $x = 0.1$ m and at the wall at $x = 0.15$ m due to buoyancy effects. Figure 2b shows H_2O mass fraction contours in the reactor. The water vapor and nitrogen gases are essentially completely mixed 0.14 m from the reactor inlet and well before the high-temperature zone. When the coflowing gas is hydrogen, calculations show that mixing occurs much faster due to hydrogen's higher diffusion coefficient and the gases are fully mixed at $x = 0.11$ m. In addition, hydrogen's lower density causes the size of the wall recirculation zone to slightly increase.

III. Experimental Results

3.1. Determination of the Most Reactive System. The experimental investigations of $Cu(acac)_2$ decomposition have been carried out in hydrogen−nitrogen, in water-nitrogen, and in water-hydrogen−nitrogen atmospheres at three furnace temperatures. The inner flow of nitrogen containing $Cu(acac)_2$ vapor is always maintained equal to $Q_{Cu(acac)_2} = 330$ cm^3/s. For the preliminary experiments, the precursor vapor pressure after the saturator is always maintained equal to $P = 6 \pm 1$ Pa. The philosophy behind the preliminary experiments is to determine the crystalline products of the decomposition and to find the most reactive system for further careful investigations. Let us separately consider the experimental results obtained in different systems.

3.1.1. Decomposition in $Cu(acac)_2-H_2-N_2$ System. The investigations were carried out in the range of hydrogen−nitrogen flow rates from $Q_{H_2/N_2} = 80$ to 1980 cm^3/s. In TEM images of collected samples produced at the lowest flow rate at $t_{furn} = 432$ °C, ultrafine copper particles with a primary particle size of approximately 7−10 nm can be found. It is worth noting that there is a layer of undecomposed precursor around the synthesized particles. A similar unreacted $Cu(acac)_2$ layer was reported in our previous study[17] at this temperature, when only 20% of the precursor was decomposed in an inert nitrogen atmosphere. TGA results for the current investigation system at $Q_{H_2/N_2} = 80$ cm^3/s revealed 47% decomposition of the precursor. Increasing the flow rate leads to an increase of the

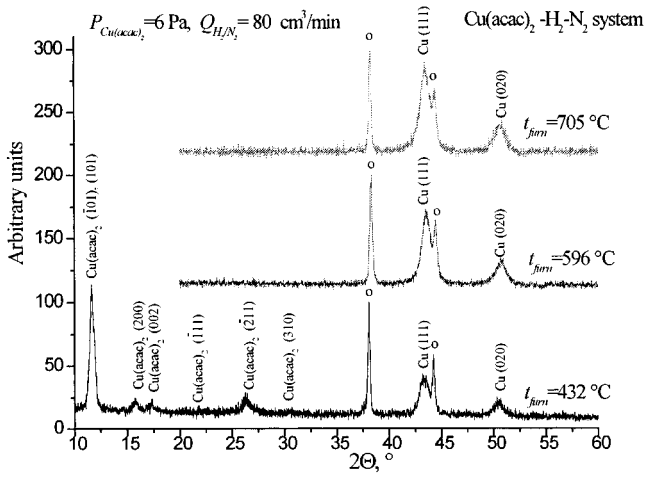

Figure 3. XRD spectra of nanoparticles synthesized at different furnace temperatures and $P_{Cu(acac)_2} = 6$ Pa with the reagent mixture flow rate of $Q_{H_2/N_2} = 80$ cm³/s in the $Cu(acac)_2-H_2-N_2$ system. The "o" marks indicate silver filter peaks.

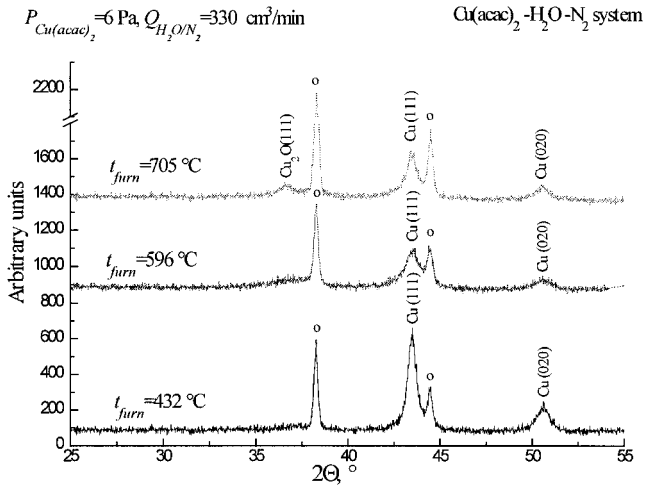

Figure 4. XRD spectra of nanoparticles synthesized at different furnace temperatures and $P_{Cu(acac)_2} = 6$ Pa with the reagent mixture flow rate of $Q_{H_2O/N_2} = 330$ cm³/s in the $Cu(acac)_2-H_2O-N_2$ system. The "o" marks indicate silver filter peaks.

amount of undecomposed precursor due to a reduced residence time in the reactor hot zone.

In Figure 3, XRD diffractograms of the particles synthesized using hydrogen as a reagent and collected on a silver filter are shown. At the lowest experimental temperature, peaks corresponding to the crystalline precursor can be seen that once again indicate incomplete $Cu(acac)_2$ decomposition at a temperature of 432 °C. It is worth noting that only crystalline copper phase is observed at higher temperatures. When compared to the $Cu(acac)_2$ decomposition in nitrogen, the introduction of hydrogen into the system prevents the appearance of copper (I) oxide at $t_{furn} = 705$ °C.

3.1.2. Decomposition in $Cu(acac)_2-H_2O-N_2$ System. For saturation of nitrogen carrier gas by water vapor, a bubbler at room temperature is used. The pressure of the water vapor after the bubbler is $P_{H_2O} = 2.7$ kPa, which corresponds to the mixture content of 97.4% nitrogen and 2.6% water.

The TGA investigations of nanoparticles synthesized at different furnace temperatures with a flow rate of $Q_{H_2O/N_2} = 330$ cm³/s and collected downstream of the furnace revealed that, at $t_{furn} = 432$ °C, about 6% of some low volatile product appears in the sample. This can be most readily explained as due to the undecomposed precursor. However, increasing the temperature in the furnace leads to a greater amount of this low volatile product, which is in contradiction to the hypothesis. As will be shown later, the decomposition at the lowest furnace temperature of $t_{furn} = 432$ °C is complete, and the low volatile material appears as a result of secondary reactions of the decomposition products. It is worth noting that the minimum temperature for complete precursor decomposition in pure nitrogen was 705 °C, while the presence of water vapor reduced this temperature to 432 °C.

XRD diffractograms of the particles synthesized using water as a reagent ($Q_{H_2O/N_2} = 330$ cm³/s) and collected on silver filter are shown in Figure 4. At the furnace temperatures of $t_{furn} = 432$ °C, only crystalline copper phase is identified. At the furnace temperatures of $t_{furn} = 596$ °C, the main crystalline product is copper, and the amount of copper (I) oxide is very small (on the same order as the sensitivity of the XRD method). At $t_{furn} = 705$ °C, the diffractogram shows the presence of both copper and copper (I) oxide phases.

3.1.3. Decomposition in $Cu(acac)_2-H_2O-H_2-N_2$ System. To check the simultaneous influence of hydrogen and water vapor, the reagent gas was obtained by bubbling the hydrogen−nitrogen mixture (7.0/93.0) through the water. The mixture percentage contents of nitrogen, hydrogen, and water after the bubbler are 91.7%, 5.7%, and 2.6%, respectively.

TABLE 1: List of Experimental Conditions and Corresponding Product Compositions (Based on XRD Analyses) of the Particles Synthesized at the Precursor Vapor Pressure of $P_{Cu(acac)_2} = 6 \pm 1$ Pa

furnace temp, °C	reagents			
	−	H_2	H_2O	H_2/H_2O
432	Cu	Cu	Cu	Cu
596	Cu	Cu	Cu[a]	Cu
705	Cu and Cu_2O	Cu	Cu and Cu_2O	Cu and Cu_2O

[a] The amount of copper (I) oxide is on the same order as the sensitivity of the XRD method

XRD analysis of the particles synthesized using hydrogen and water vapor as reagents found the same crystalline phase dependence on temperature as if only water vapor were used as a reagent (Figure 4). At the furnace temperatures of $t_{furn} = 432$ and 596 °C, only crystalline copper phase is identified, and a mixture of copper and copper (I) oxide is found at the temperature of 705 °C. A quantitative XRD analysis shows that the presence of hydrogen in the system decreased the amount of copper (I) oxide by a factor of 2. However, the influence of hydrogen on the crystalline product is not significant because introducing hydrogen into the system does not lead to the prevention of copper oxide formation.

3.1.4. Conclusion of the Preliminary Experimental Results. The experimental conditions and corresponding product compositions identified by XRD analyses are presented in Table 1. It can be seen that the presence of the reagent does not significantly affect on the products of the decomposition. The exception is the decomposition in the $Cu(acac)_2-H_2-N_2$ system at $t_{furn} = 705$ °C, where only copper phase was identified in the product. For other systems at the highest temperature, a mixture of copper and copper (I) oxide was found. It is worth noting that the presence of a reagent, as a rule, decreases the furnace temperature at which complete precursor decomposition occurs. The complete reaction of $Cu(acac)_2$ decomposition in inert nitrogen occurred at $t_{furn} = 705$ °C. In the presence of hydrogen, this temperature is decreased to 596 °C. But the most drastic effect is observed after the introduction of the water vapor into the system. This case, the temperature of complete decomposition is reduced to 432 °C.

EDS spectra of nanoparticles synthesized at the furnace temperature of 432 °C with different reagents are shown in Figure 5. From the figure, one can see that a carbon peak exists with particles synthesized using pure nitrogen or hydrogen−nitrogen carrier gas. The presence of water significantly decreased the presence of impurities on the particles.

Thereby, when compared to the decomposition in various systems, it can be inferred that the most reactive conditions appeared after the water introduction into system. Simultaneous usage of water and hydrogen increases the number of independent variables in the system, complicates the experimental control, and does not give any practical benefits. Neither a significant increase of the decomposition rate nor a influence on the decomposition product at $t_{furn} = 432$ °C was observed. Thus, our further studies will be directed on the investigation of decomposition and nanoparticle formation in the $Cu(acac)_2-H_2O-N_2$ system.

3.2. Investigation of the Decomposition in the $Cu(acac)_2-H_2O-N_2$ System. *3.2.1. Mechanistic Studying the Precursor Decomposition.* Studies of the mechanism of the $Cu(acac)_2$ precursor decomposition in the presence of water vapor were carried out at $t_{furn} = 432$ °C and a precursor vapor pressure of 6 Pa. At this condition, the main crystalline product was copper. Gas chromatography mass spectrometry (GC-MS) investigations of the gas phase downstream of the furnace were carried out. On the basis of the experimental results, a conceptual mechanism of $Cu(acac)_2$ decomposition is proposed.

Experimental results show that the presence of water vapor in the system considerably decreased the precursor decomposition temperature. It affords ground for a suggestion of formation of the hydrate complex that is less stable compared to the anhydride compound.[18] Apparently, the formed bond between the oxygen of water molecules and copper plays a very important role in weakening the ligand−metal bond. A proton from the coordinated water molecule transfers to the ligand,[18] which is freed in the form of gaseous acetylacetone (2,4-pentadione):

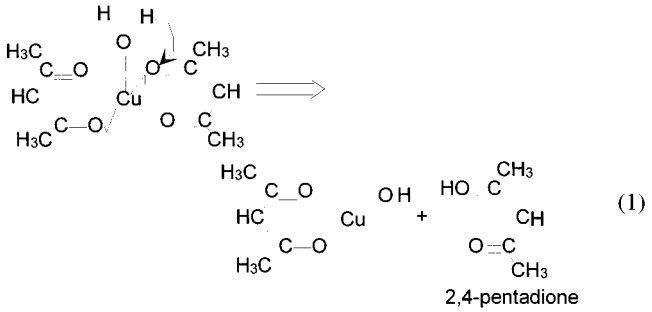

(1)

The reduction of Cu^{2+} to Cu^0 should occur at the expense of ligand oxidation, which occurs according to eq 2. Some of the ligands are liberated as 2,4-pentadione existing in the enol form on 92−93% in the gas phase.[21] The rest of the ligands are oxidized, thus forming acetone, acetic acid, and carbon dioxide.

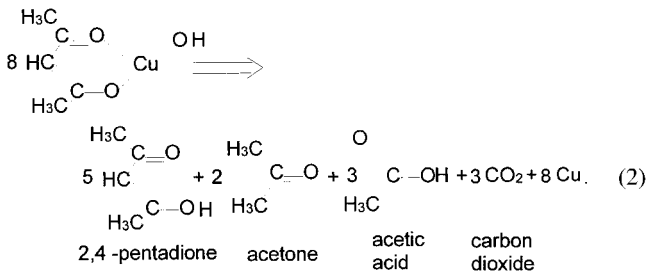

(2)

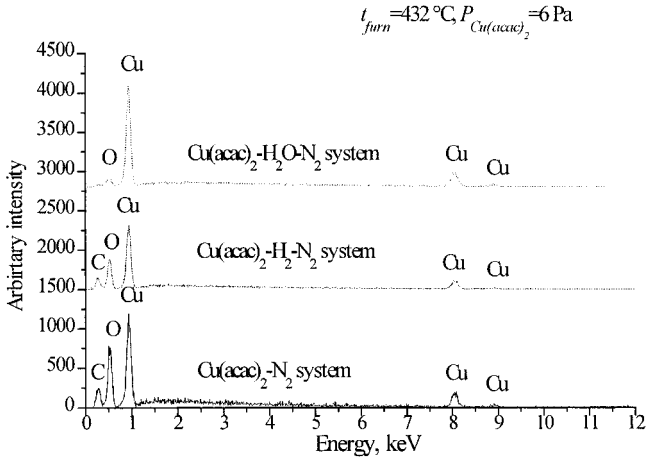

Figure 5. EDS spectra of nanoparticles synthesized at furnace temperature of 432 °C in the different systems.

The stoichiometric coefficients for the reaction eq 2 were obtained on the basis of the GC-MS results of the reaction product contents. As a free fitting parameter to equalize the equation, the concentration of carbon dioxide, which was not precisely determined, has been used.

It is important that the presence of a small amount (6%) of some low volatile products were determined by TGA at a $Cu(acac)_2$ vapor pressure of $P_{Cu(acac)_2} = 6$ Pa. TGA results of nanoparticles synthesized at different furnace temperatures showed that the amount of this unknown low volatile substances increased with increasing the temperature. Comparing the experimental TGA curves and $Cu(acac)_2$ standard curve revealed the absence of the precursor in the collected sample. The black color of the collected particles allows us to make the same conclusion, since, in the presence of undecomposed $Cu(acac)_2$, the sample becomes blue. Information about the formation of this low volatile compound can be obtained from the IR analysis of the layer around the particles. To analyze the composition of the layer around the collected nanoparticles, they were placed in a solvent (toluene) and heated to 50 °C for 1 h. TEM micrographs of the particles after this procedure showed that the layer had been almost completely dissolved in the toluene. Then the filtered solution was evaporated, and a residue was analyzed by IR methods described earlier. The IR spectra obtained from the layers around the nanoparticles synthesized with different reagents at 705 °C are presented in Figure 6. For comparison, a precursor IR spectrum is also shown in the figure. It is obvious that the examined material could not be the precursor.

The detail analysis of the IR spectra peaks is presented in Table 2. As one can see, the particles are covered by a complicated organic substance (or a mixture of substances). This organic material most likely contains long chain alkane groups (722 cm^{-1}), primary and secondary alcohols (1037 cm^{-1}, 1118 cm^{-1}, 1278 cm^{-1}, 3390−3450 cm^{-1}), ester (1117 cm^{-1}, 1735 cm^{-1}), ether (1074 cm^{-1}), and ketone (1614 cm^{-1}) groups. The experimental IR spectrum for the $Cu(acac)_2-H_2O-N_2$ system fits quite well with that of (*E*)-9-octadecenoic acid ethyl ester (see Figure 7). The difference is in the peak at the wavenumber of 1614 cm^{-1}, corresponding to the presence of β-diketonate group in the sample. The mechanism of formation of such compound is not clear as yet. The presence of ketone, alcohol (e.g., acetylacetone), and carboxyl acid representatives in the gas phase could lead to a variety of different reactions; for example, aldol condensation, nucleaphilic addition, or the formation of ketals could also take place. The products of the

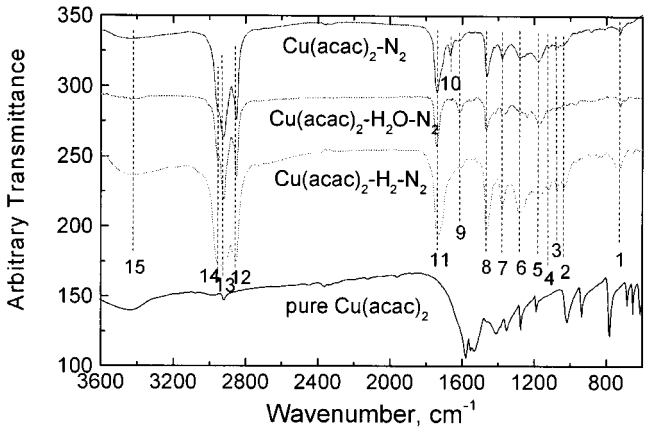

Figure 6. Traces showing the infrared spectra obtained from the layer around nanoparticles produced without any reagent, with water, and with hydrogen. The bottom spectrum corresponds to pure $Cu(acac)_2$. Nanoparticles were synthesized at $t_{furn} = 705$ °C and $P_{Cu(acac)_2} = 6$ Pa.

last reaction were found in the gas phase in small quantities (about 2%). It is well-known that copper is a very good catalyst for many organic reactions. The presence of high surface area copper in the gas phase might catalyze the mentioned reactions.[22,23] Apparently, catalytic surface reactions for the decomposition organic products occur on the formed copper particles. Accordingly, such a great variety of probable reactions makes schematic chemical presentation for the reaction pathway difficult.

3.2.2. Nanoparticle Formation. TEM micrographs of the nanoparticles synthesized at $t_{furn} = 432$ °C and different precursor vapor pressures are presented in Figure 8. At the precursor vapor pressures of $P_{Cu(acac)_2} = 1$ Pa, the crystalline qualitative analysis of the collected nanoparticles was carried out by XRD analysis and from electron diffraction patterns. The particle phase identification at lower precursor vapor pressures was performed by using electron diffraction and high-resolution TEM images. It was found that at the furnace temperature of 432 °C decreasing $P_{Cu(acac)_2}$ changed crystalline products from copper to copper (I) oxide. In Figure 9, an example of a high-resolution TEM image of a particle synthesized at a precursor vapor pressure of $P_{Cu(acac)_2} = 0.07$ Pa is presented. This particle was identified as Cu_2O on the basis of the crystallographic data. Similarly, only the pure copper (I) oxide crystalline phase was found at $P_{Cu(acac)_2} = 0.13$ Pa. At the precursor vapor pressure of $P_{Cu(acac)_2} = 1.9$ Pa, the mixture of both copper and copper (I) oxide phases was found. At the precursor vapor pressure of $P_{Cu(acac)_2} = 6$ Pa, only copper crystalline phase was identified by XRD analysis, and a very small amount of copper (I) oxide was determined from electron diffraction patterns of collected particles; i.e., the Cu_2O mole crystalline fraction is smaller than the sensitivity of the XRD analysis. Thus, the influence of the precursor concentration on the crystalline phase of the products has been determined. The possible reason for the phenomena are discussed in the next part of this article.

From Figure 8, one can see that the particles are agglomerated at the precursor vapor pressure of $P_{Cu(acac)_2} = 6$ and 1.9 Pa and become single unagglomerated particles at $P_{Cu(acac)_2} = 0.13$ Pa. In Figure 10, the normalized primary particle size distributions obtained from TEM images and DMA measurements are presented. The size of the primary particles is dependent on the precursor vapor pressure; the geometric mean diameter of $D_p = 27.3$ nm (with geometric standard deviation of $\sigma_g = 1.34$) at $P_{Cu(acac)_2} = 6$ Pa, $D_p = 15.6$ nm ($\sigma_g = 1.35$) at $P_{Cu(acac)_2} = 1.9$ Pa, $D_p = 5.2$ nm ($\sigma_g = 1.33$) from TEM images and $D_p = 6.1$ nm ($\sigma_g = 1.35$) from DMA measurements at $P_{Cu(acac)_2} = 0.13$ Pa, and $D_p = 4.2$ nm ($\sigma_g = 1.19$) from DMA measurements at $P_{Cu(acac)_2} = 0.07$ Pa. The small value of the geometric standard deviation for the last case could be explained by low count efficiency of the CPC for particles smaller than 5 nm. The comparison made for TEM and DMA results at $P_{Cu(acac)_2} = 0.13$ Pa found a difference (about 15%) between these two methods. Since the DMA system gives the number size distribution of all particles, the difference can be caused by the partial agglomeration of primary particles. Also, it is known[24,25] that the DMA system gives oversized number size distribution for nanometer size range.

IV. Discussion

The experimental results (Table 1, Figure 8) revealed the dependencies of the crystalline products on the temperature and the precursor vapor pressure. At low temperatures and at the precursor vapor pressure of $P_{Cu(acac)_2} = 6$ Pa, the main crystalline product was copper. Increasing the temperature in the system leads to the appearance of a second crystalline product—copper (I) oxide. At the furnace temperature of $t_{furn} = 432$ °C, the formation of copper (I) oxide particles occurs by decreasing the precursor vapor pressure.

It is obvious that the formation of the copper (I) oxide phase in the absence of molecular oxygen can be explained only as a reaction of copper vapor and oxygen containing species. The possible oxidizers in the system can be water or products of the decomposition (e.g., carbon dioxide). The possibility of copper oxidation via H_2O and CO_2 is justified from the thermodynamic point of view:

$$2Cu(g) + H_2O(g) \leftrightarrow Cu_2O(s) + H_2(g), \quad \Delta G_{432} = -398 \text{ and } \Delta G_{705} = -319 \text{ kJ/mol} \quad (3)$$

$$2Cu(g) + CO_2(g) \leftrightarrow Cu_2O(s) + CO(g), \quad \Delta G_{432} = -385 \text{ and } \Delta G_{705} = -323 \text{ kJ/mol} \quad (4)$$

where ΔG_t is a change of a free energy of the reaction at temperature t.

Detailed consideration of the formation of the different phases and the kinetics of the particle growth will not be discussed here. It has been considered thoroughly in our earlier papers.[26,28] Let us discuss only the possibility of a qualitative explanation of the experimental results based on thermodynamic predictions of the crystalline products. The thermodynamic calculations were carried out using the FACT software[29] at system temperatures of 432 and 705 °C for the experimental $Cu(acac)_2$–H_2O–N_2 system. The results of the calculations of solid Cu_2O mole fraction dependence on the ratio of water and copper pressures are presented in Figure 11. It is necessary to note that the influence of carbon dioxide on the crystalline products was neglected because of the very high water concentration. For the calculations, a fixed experimental water vapor pressure of $P_{H_2O} = 2.7$ kPa was used, and copper vapor pressure was chosen as a variable parameter.

From the results presented in Figure 11, the qualitative explanation of the crystalline product dependencies on temperature and precursor vapor pressure can be obtained. First, let us consider the influence of the furnace temperature on the crystalline phase at the precursor vapor pressure of $P_{Cu(acac)_2} = 6$ Pa. At $t_{furn} = 432$ °C, the main product was copper. The Cu_2O phase presence was identified only from the electrondiffraction patterns, implying that the amount of copper (I) oxide is less than 1%, i.e., less than the sensitivity of the XRD method. At

TABLE 2: Infrared Mode Description of the Spectra Presented in the Figure 6

no.	wavenumber, cm^{-1}	mode description: bonds	mode description: compound class
1	722	C−C, skeletal, in-phase rock	alkanes, $(CH_2)_n$, for $n > 4$
2	1037	C−O, str.	primary alcohols (R−OH)
3	1074	C−O−C, asym. str.	ethers (R−O−R′)
4	1118	C−O, str.	secondary alcohols (R−OH−R′)
5	1170	C−O, str.	esters (R−CO−O−R′)
6	1278	C−O, def.	primary and secondary alcohols (R−OH) and (R−OH−R′)
7	1377	C−H, asym. def., C−H, def.	alkanes (R−CH_3), alkanes (R−CH_2−)
8	1462	C−H, def.	alkanes (R−CH_2−)
9	1614	C═O, str.	β-diketonates (R−CO−CH2−CO−R′)
10	1664	C═O, str.	unsaturated ketones (R−CH═CH−CO−R′)
11	1735	C═O, str.	esters, (R−CO−O−R′)
12	2852	C−H, sym. str.	alkanes (R−CH_2−)
13	2922	C−H, asym. str.	alkanes (R−CH_2−)
14	2954	C−H, asym. str.	alkanes (R−CH_3)
15	3390−3450	O−H, str.	compounds containing (−OH) group

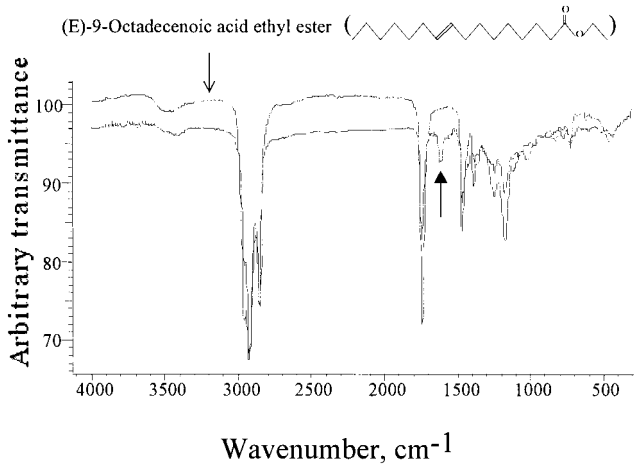

Figure 7. Comparison of IR curves of (*E*)-9-octadecenoic acid ethyl ester standard and the experimental sample produced in the $Cu(acac)_2$−H_2O−N_2 system.

$t_{furn} = 705$ °C, the Cu_2O percentage content in the solid is about 10% according to the quantitative XRD analysis (Figure 4). Thus, increasing the temperature from 432 °C to 705 °C leads to an increase of the Cu_2O concentration by a factor of more than 10. The same behavior can be inferred from the thermodynamic calculations at a given copper vapor pressure: the copper (I) oxide mole fraction at $t_{furn} = 705$ °C is almost 2 orders of magnitude higher than at $t_{furn} = 432$ °C.

The explanation of the solid product change on the precursor vapor pressure at the furnace temperature of 432 °C can be also found from Figure 11. One can see that the crystalline products are very strongly dependent on the ratio of the reagents. From the experiments, it was found that copper phase was formed at $P_{Cu(acac)_2} = 6$ Pa and the Cu_2O phase at $P_{Cu(acac)_2} = 0.13$ Pa. Thus, varying the precursor vapor pressure by a factor of 45 changes the solid product phase from essentially pure copper to essentially pure copper (I) oxide. In an equilibrium system, for the formation of the pure Cu and Cu_2O phases, the copper pressure should be equal to $P_{Cu} = 5 \times 10^{-2}$ and 10^{-3} Pa, respectively; i.e., a product change from Cu to Cu_2O occurs within a 1.5 order of magnitude change in the copper vapor concentration.

Also, it is worth noting that kinetic considerations of copper oxidation have not be taken into account. It is known that the crystalline product formation is determined by the ratio of copper-containing and water vapor fluxes on the growing particle, exceeding the certain activation energy barrier. If the copper flux is much higher than water, then conditions favoring copper particle formation appears.[26] The water concentration and, hence, the flux (if we do not take into account the temperature gradient) are maintained at a constant value and do not depend on the precursor vapor pressure. The copper vapor pressure, and thus the flux, however, varied along the reactor tube. The copper concentration is constantly changing at the expense of precursor decomposition, vapor nucleation, and the

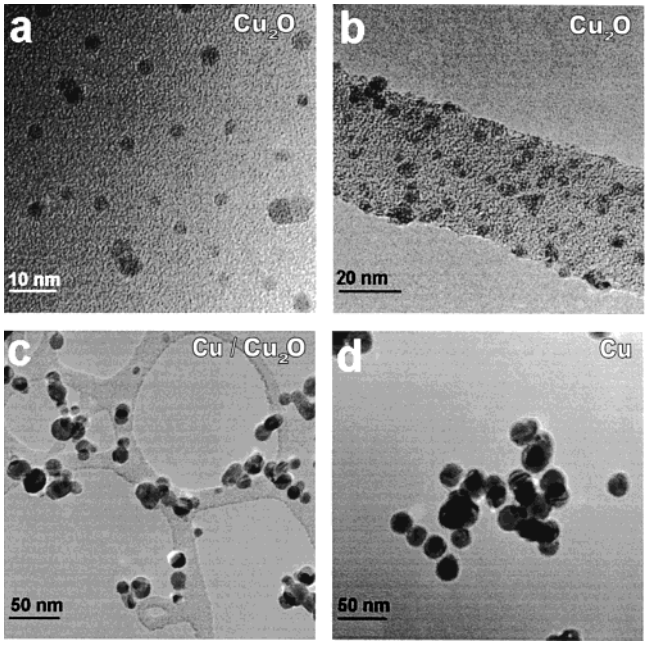

Figure 8. Transmission electron micrographs of particles produced at $t_{furn} = 432$ °C in the $Cu(acac)_2$−H_2−N_2 system. Precursor vapor pressure, $P_{Cu(acac)_2}$: (a) 0.07, (b) 0.13, (c) 1.9, and (d) 6 Pa.

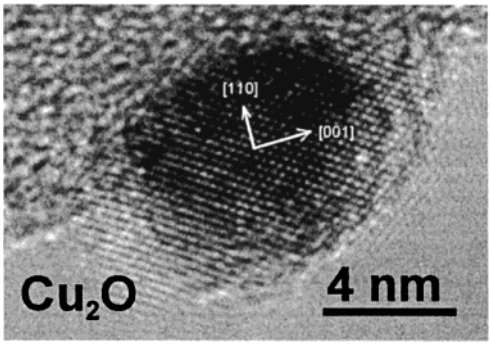

Figure 9. High-resolution TEM picture of a Cu_2O particle synthesized at the furnace temperature 432 °C and with precursor vapor pressure of $P_{Cu(acac)_2} = 0.07$ Pa.

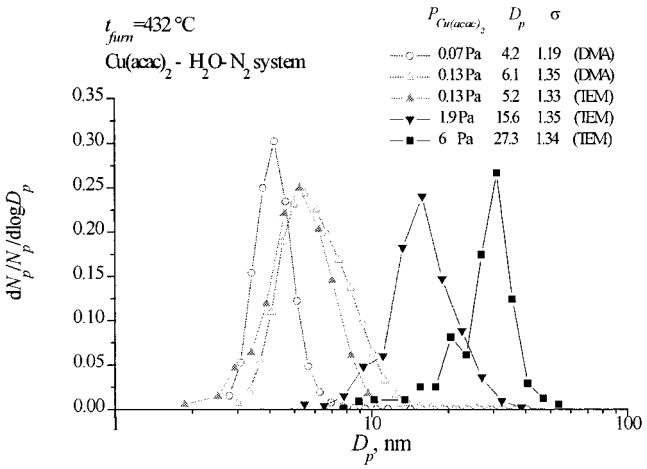

Figure 10. Normalized number size distribution of primary particles synthesized in the $Cu(acac)_2-H_2O-N_2$ system.

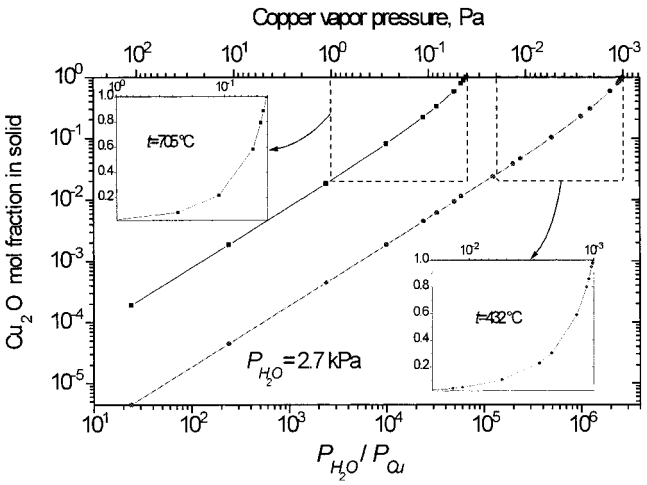

Figure 11. Dependence of crystalline products on the ratio of water and copper vapor pressures. The thermodynamic calculations were carried out at fixed experimental water vapor pressure of $P_{H_2O} = 2736$ Pa and for two temperatures of 432 °C and 705 °C.

condensation processes. Apparently, the copper vapor pressure in the region of growing particle is much less than the total precursor vapor pressure. This explains that the difference in the Cu_2O formation conditions between the thermodynamic calculations ($P_{Cu} = 10^{-3}$ Pa) and the experimental value of vapor pressures ($P_{Cu(acac)_2} = 0.13$ Pa), when only Cu_2O forms, is almost 2 orders of magnitude. This value seems to be realistic on the basis of computational fluid dynamic calculations of the decomposition reactions inside the reactor.[30]

As for other experimental systems, a similar qualitative explanation of the change of the crystalline products can be also obtained on the basis of the consideration of the processes occurring inside the reactor. In the $Cu(acac)_2-N_2$ system at 705 °C,[26] the copper (I) oxide phase appears because of the presence of carbon dioxide and water vapor, which are the decomposition products.[31] The prevention of the Cu_2O formation could be realized by introducing hydrogen into the system where, according to Le Chatelier's principle, the reaction 3 is tipped toward formation of the pure copper phase. But it was experimentally found that the presence of hydrogen in the system did not lead to complete prevention of Cu_2O formation and the amount of the oxide was decreased by a factor of 2 (see the results for $Cu(acac)_2-H_2-H_2O-N_2$ system). Thus, the influence of hydrogen on the crystalline product is not significant.

Conclusion

The experimental investigations of copper (II) acetylacetonate vapor decomposition and subsequent copper and copper (I) oxide particle formation were studied in a vertical laminar flow reactor in the presence of hydrogen and water vapor in a nitrogen atmosphere. It was found that the presence of hydrogen did not significantly affect on the decomposition rate. The most reactive conditions for the precursor decomposition appeared when water vapor were introduced into the system. A mechanism for $Cu(acac)_2$ decomposition in the presence of water has been proposed. The reaction pathway can be divided into three steps: a formation of gaseous hydrate complex; a proton transition from the coordinated water to a ligand and a further liberation in the form of gaseous acetylacetone; the partial destruction (oxidation) of the resulting ligands and a reduction reaction of Cu^{2+} to Cu^0. The formation of copper particles leads to a surface catalytic reaction of the organic decomposition products. As a result of this reaction, low-volatility long-chain compounds containing ketone, alcohol, ester, and ether groups were formed. The crystalline product depends on the system temperature and precursor vapor pressure. The crystallinity of the formed particles was changed from copper to copper (I) oxide when the precursor vapor pressure was decreased from $P_{Cu(acac)_2} = 6$ to 0.13 Pa at $t_{furn} = 432$ °C and the temperarture was increased to $t_{furn} = 705$ °C at $P_{Cu(acac)_2} = 6$ Pa. A qualitative thermodynamic explanation of the change of crystalline phases is proposed.

Primary particle size distributions at $t_{furn} = 432$ °C were measured from TEM images. The size of the particles is dependent on the precursor vapor pressure; the geometric mean diameter of $D_p = 27.3$ nm (with geometric standard deviation of $\sigma_g = 1.34$) at $P_{Cu(acac)_2} = 6$ Pa, $D_p = 15.6$ nm ($\sigma_g = 1.35$) at $P_{Cu(acac)_2} = 1.9$ Pa, $D_p = 5.2$ nm ($\sigma_g = 1.33$) from TEM images and $D_p = 6.1$ nm ($\sigma_g = 1.35$) from DMA measurements at $P_{Cu(acac)_2} = 0.13$ Pa, and $D_p = 4.2$ nm ($\sigma_g = 1.19$) from DMA measurements at $P_{Cu(acac)_2} = 0.07$ Pa.

Acknowledgment. This work has been supported by TEKES, Finland, and VTT Chemical Technology via the MATRA research program. We thank Dr. O. Richard for supervising the TEM work. Mr. H. Risto and Mr. Erik Sandell are acknowledged for carrying out IR and GC-MS analyses. Mr. P. Räisanen, Dr. M. Ritala, and Prof. M. Leskelä are gratefully acknowledged for help during the XRD-analyses and Mr. T. Hatanpää for carrying out TGA analysis.

References and Notes

(1) Sievers, R. E.; Sadlowski, J. E. *Science* **1978,** 201, 217.
(2) Kodas, T. T.; Hampden-Smith, M. J. *The Chemistry of Metal CVD*; VCH: Weinheim, Germany 1994.
(3) Kanapilly, G. M.; Tu, K. W.; Larsen, T. B.; Fogel, G. R.; Luna, R. J. *J. Colloid Interface Sci.* **1978**, *65*, 553.
(4) Slootman, F.; Parent, J.-C. *J. Aerosol Sci.* **1994**, *25*, 15.
(5) Onischuk, A. A.; Strunin, V. P.; Ushakova, M. A.; Panfilov, V. N. *J. Aerosol Sci.* **1997**, *28*, 207.
(6) Majumdar, D.; Shefelbine, T. A.; Kodas, T. T.; Glicksman, H. D. *J. Mater. Res.* **1996**, *11*, 2861.
(7) Holzschuh, H.; Suhr, H. *Appl. Phys.* **1990**, A51, 486.
(8) Campbell, C. T.; Daube, K. A.; White, J. M. *Surf. Sci.* **1987**, *182*, 458.
(9) Du, F.-L.; Cui, Z.-L.; Zhang, Z.-K.; Chen, S.-Y. *J. Nat. Gas Chem.* **1997**, *6*, 135.
(10) Klier, K. *Adv. Catal.* **1982**, *31*, 243.
(11) Pauleau, Y.; Fasasi, A. Y. *Chem. Mater.* **1991**, *3*, 45.
(12) Gerfin, T.; Becht, M.; Dahmen, K.-H. *Mater. Sci. Eng.* **1993**, B17, 97.
(13) Hammadi, Z.; Lecohier, B.; Dallaporta, H. *J. Appl. Phys.* **1993**, *73*, 5213.

(14) Maruyama, T.; Shirai, T. *J. Mater. Sci.* **1995**, *30*, 5551.
(15) Okuyama, K.; Shimada, M.; Adachi, M.; Tohge, N. *J. Aerosol Sci.* **1993**, *24*, 357.
(16) Daróczi, L.; Beck, M. T.; Beke, D. L.; Kis-Varga, M.; Harasztosi, L.; Takacs, N. *Mater. Sci. Forum* **1998**, 269−272, 319.
(17) Nasibulin, A. G.; Ahonen, P. P.; Richard, O.; Kauppinen, E. I.; Brown, D. P.; Jokiniemi, J. K. *Book of Abstracts of Second Joint ESF-NSF 1999 Symposium on "Nanoparticles: Technologies and Applications"*, Tacoma, WA, Oct 10, 1999; Gerhard-Mercator University: Duisburg, Germany, 1999.
(18) Pinkas, J.; Huffman, J. C.; Baxter, D. V.; Chisholm, M. H.; Caulton, K. G. *Chem. Mater.* **1995**, *7*, 1589.
(19) Winklmayr, W.; Reischl, G. P.; Linder, A. O.; Berner, A. *J. Aerosol Sci.* **1991**, *22*, 289.
(20) Brown, D. P. *NIST SBIR 97-1-58 Final Rep.* **1998**.
(21) Mines, G. W.; Thompson, H. *Proc. R. Soc. London, Ser. A* **1975**, *342*, 327.
(22) Dhas, N. A.; Raj, C. P.; Gedanken, A. *Chem. Mater.* **1998**, *10*, 1446.
(23) Morrison, R. T.; Boyd, R. N. *Organic Chemistry*; Allyn & Bacon: Boston, 1975.
(24) Deppert, K.; Bovin, J.-O.; Malm, J.-O.; Samuelson, L. *J. Cryst. Growth* **1996**, 169, 13.
(25) Kuga, Y.; Ando, K.; Okuyama, K.; Takeuchi, K. *J. Aerosol Sci.* **1999**, Suppl. 1, 347.
(26) Nasibulin, A. G.; Ahonen, P. P.; Richard, O.; Kauppinen, E. I.; Altman, I. S. *J. Nanoparticle Res.*, in press.
(27) Petrov, Yu. I. *Clusters and Small Particles* (*Klastery i Malye Chastitcy*, in Russian); Nauka: Moscow, 1986.
(28) Nasibulin, A. G.; Richard, O.; Kauppinen, E. I.; Brown, D. P.; Jokiniemi, J. K.; Altman, I. S. *Aerosol Sci. Technol.*, submitted for publication.
(29) Bale, C. W.; Pelton, A. D. ≪*Fact-Win*≫ - *User-Manual*; École Polytechnique de Montréal Québec: Montréal, Canada, 1999.
(30) Brown, D. P.; Nasibulin, A. G.; Kauppinen, E. I.; Jokiniemi, J. K. Abstract of International Congress for Particle Technology "PARTEC 2001"; Nürnberg, Germany 27−29 March, 2001; International Congress for Particle Technology: Nürnberg, 2001; p 107.
(31) Tsyganova, E. I.; Mazurenko, G. A.; Drobotenko, V. N.; Dyagileva, L. M.; Aleksandrov, Yu. A. *Zh. Obshch. Khim.* **1992**, *62*, 499 [*J. Gen. Chem.* **1992**, 62, 407].